

Projected changes of the Northern Annular Mode linked to seasonality of the ENSO teleconnection

T. Kawamura¹, Y. Kosaka¹, S. Okajima¹, and H. Nakamura¹

¹Research Center for Advanced Science and Technology, the University of Tokyo, Japan

Corresponding author: Takashi Kawamura (tkawamura@atmos.rcast.u-tokyo.ac.jp)

Key Points:

- The proportion of the Northern Annular Mode variance driven by variability of sea surface conditions increases in the warmer climate.
- This change is tied to early-winter emergence of the Aleutian-Icelandic Low seesaw which is limited to late winter in the present climate.
- Teleconnection from the El Niño-Southern Oscillation contributes to the earlier winter emergence of the seesaw in the warmer climate.

Abstract

The Northern Annular Mode (NAM) is the dominant pattern of atmospheric circulation variability in the wintertime Northern Hemisphere extratropics. This study utilizes a large ensemble atmospheric simulation dataset to examine the seasonality of the NAM variability and its modulations under global warming. We show an enhancement of the Aleutian Low anomaly associated with the NAM in a warmer climate. This enhancement is related to the emergence of the Aleutian-Icelandic Low seesaw (AIS) from early winter, which is in contrast prominent only in late winter in the historical climate. The large ensemble reveals a significant increase in the fraction of the NAM variance explained by sea surface temperature and sea ice variability, suggesting a higher potential predictability. In particular, the eastward extension of the El Niño-Southern Oscillation (ENSO) teleconnection under global warming contributes to the AIS formation even in early winter and a higher NAM-ENSO correlation.

Plain Language Summary

Anomalous weather in the wintertime Northern Hemisphere extratropics is linked to the Northern Annular Mode (NAM). It manifests as the seesaw-like air pressure anomalies between the Arctic region and the midlatitude ocean basins. Despite its importance for climate risk assessment in a warming world, future changes in the year-to-year NAM variability have not been sufficiently investigated. Based on a large ensemble atmospheric simulation dataset of over 10,000 model years, we show that the NAM in a warmer climate correlates more tightly with the El Niño-Southern Oscillation, a dominant climate mode over the tropical Pacific. Our finding suggests a higher potential predictability of the NAM under global warming.

1 Introduction

The Northern Annular Mode (NAM), also known as the Arctic Oscillation, is the most dominant pattern of atmospheric circulation variability in the wintertime Northern Hemisphere extratropics (Thompson & Wallace, 1998). The NAM features the same-signed sea-level pressure (SLP) anomalies around the climatological Aleutian Low (AL) and Azores High, and the opposite-signed SLP anomaly around the climatological Icelandic Low (IL). The two Atlantic lobes constitute the North Atlantic Oscillation (NAO), the dominant mode of variability in the North Atlantic. The NAM is also related to the strength of the polar vortex and represents a mode of variability extending from the troposphere to the stratosphere (Baldwin & Dunkerton, 1999; Kidston et al., 2015; Thompson & Wallace, 2000). Given the broad NAM influence on the surface climate (Thompson & Wallace, 1998; He et al., 2017; Thompson & Wallace, 2000), understanding its mechanisms is crucial for regional climate variability, extremes, and their seasonal forecasts.

Since identified by Thompson & Wallace (1998), the physical nature of the NAM has been debated. The main issue is its relationship with the NAO. The NAM spatially resembles the NAO in the North Atlantic sector, with a high temporal correlation between their indices. Wallace (2000) argued that the difference lies in whether one views the phenomenon locally (NAO) or hemispherically (NAM), as they are essentially the same. However, other studies questioned statistical (Deser 2000) and physical (Ambaum et al., 2001) linkages of the AL center

of action with the NAO. Among others, Honda & Nakamura (2001) discovered a prominent seesaw-like variability, named the Aleutian-Icelandic low seesaw (AIS), between the AL and IL during late winter. They suggested that the spatial pattern of the NAM is a result of the artificial mixing of the NAO and AIS through the empirical orthogonal function (EOF) analysis.

Climate model simulations suggest that the NAM shifts towards a more positive phase with global warming (Lee et al., 2021). However, aside from the mean state changes of the NAM, modulations of the statistical properties of NAM as an interannual variability remain to be elaborated further. In particular, its relationship with the AIS, which emerges in late winter in the present climate, as well as the spatial structure and amplitude of the NAM itself, have not been thoroughly investigated. In this study, we examine changes in these aspects under global warming using a large ensemble global atmospheric simulation dataset.

2 Data and Methods

2.1 Data

We use the database for Policy Decision making for Future climate change (d4PDF). d4PDF is a large ensemble of simulations by an atmospheric general circulation model (AGCM), MRI-AGCM3.2, with a 60 km horizontal resolution (Mizuta et al., 2017). The historical experiment (“HIST”) consists of 100-member ensemble simulations from 1951 to 2011, driven by observed sea surface temperatures (SST), sea ice, and external forcing factors such as greenhouse gases. d4PDF also includes a 90-member ensemble of global warming experiment (“+4K”), where the global mean surface temperature is increased to the 4°C global warming level. The SST imposed to +4K is derived by first removing the linear trend from the observations used for HIST, then adding climatological mean changes to match the global warming level. The spatial patterns of mean SST changes are derived from six selected models (Figure S1) of the Coupled Model Intercomparison Project Phase 5 (CMIP5; Taylor et al., 2012). The sea ice is also adjusted accordingly. The external forcing factors are based on the RCP8.5 scenario in the year 2090. For each of the six warming patterns, 15 ensemble simulations were conducted, comprising a 90-member ensemble of the +4K experiment. Note that interannual variability of SST is unchanged between HIST and +4K. All the data has been interpolated to 1.25-degree horizontal resolutions.

In d4PDF, small perturbations within the range of observational errors have been added to the prescribed SST, which differ among ensemble members. In this study, we disregard this influence and evaluate the variability of the ensemble mean as the component driven by SST and sea ice variability.

As a reference, we use the ERA5 reanalysis data (Hersbach et al., 2020) from 1940 to 2022 with a 1-degree horizontal resolution. Monthly SST data of COBE-SST2 (Hirahara et al., 2014), which served as the lower boundary condition for d4PDF, is also used for the period 1951-2011 with a horizontal resolution of 1 degree.

2.3 Analysis methods

Monthly climatology is calculated over the entire period (of the ensemble mean) of each dataset/experiment, and anomalies are defined as deviations from the monthly climatology. In

the +4K experiment, anomalies are defined relative to the climatology of individual warming patterns. Following Thompson & Wallace (1998), an EOF analysis is performed on interannual variability of monthly sea-level pressure (SLP) in the Northern Hemisphere extratropics (20–90°N). This EOF analysis is applied separately to the December–February (DJF) average and each calendar month from November to March. The NAM index is defined as the standardized first principal component time series. For d4PDF HIST (+4K), unless noted otherwise, the NAM index is defined for the variability over 6,000 (5,400) years, combining all ensemble members. The statistical significance is tested using *t*-test, with the effective degree of freedom estimated according to Bretherton et al. (1999).

3 Results

3.1 Seasonality in the NAM and its change in a warmer climate

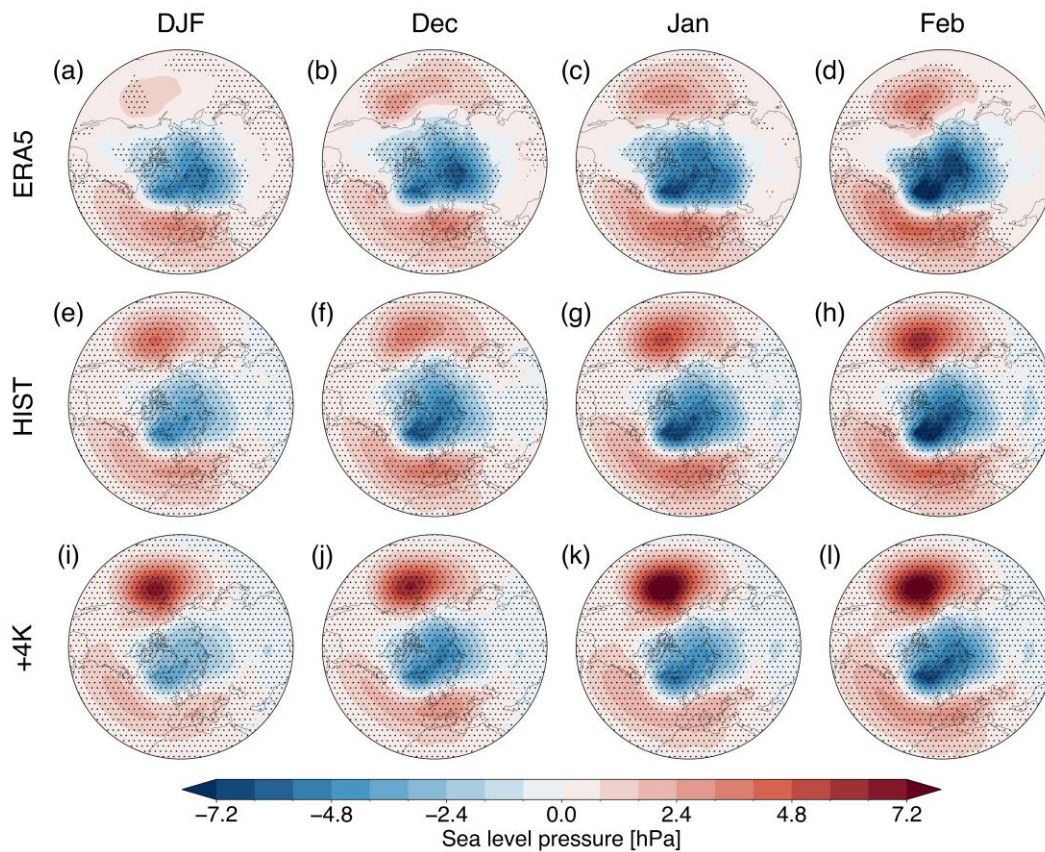


Figure 1. SLP anomalies (hPa) regressed onto the NAM index for (a) DJF-mean, (b) December, (c) January, and (d) February based on ERA5 dataset. (e–h) and (i–l) are the same as (a–d), but for d4PDF HIST and +4K, respectively. Dots indicate the statistical significance at the 95% level.

Figure 1 summarizes the SLP anomalies associated with the NAM. d4PDF reproduces the overall structure and magnitude of the NAM reasonably well (Figure 1a–h). While d4PDF overestimates the AL anomaly, as also found in a majority of CMIP5 (Gong et al., 2017; Zuo et al., 2013) and CMIP6 (Coburn & Pryor, 2021) models, it successfully captures the observed

temporal correlations among three centers of action, namely the AL and two Atlantic lobes (results not shown).

In both ERA5 and d4PDF HIST, the NAM exhibits an enhancement of the AL anomaly from early to late winter. Indeed, the ratio of squared SLP anomaly over the AL region ($40^{\circ}\text{--}55^{\circ}\text{N}$, $180^{\circ}\text{--}150^{\circ}\text{W}$) to that of the North Atlantic sector ($20^{\circ}\text{--}90^{\circ}\text{N}$, $90^{\circ}\text{W}\text{--}40^{\circ}\text{E}$) increases from December to February (1.3 times for ERA5 and 2.3 times for d4PDF). This result is qualitatively unchanged against slight changes in the AL and North Atlantic domains.

In +4K, the NAM structure becomes more Pacific-weighted (Hamouda et al., 2021). Indeed, while the SLP anomaly magnitudes at the Arctic and North Atlantic anomaly centers do not change so much from the HIST experiment, the AL anomaly of the NAM in +4K strengthens throughout winter (Figures 1i-l). As in HIST, the intensified AL anomaly also undergoes intraseasonal strengthening from December to February.

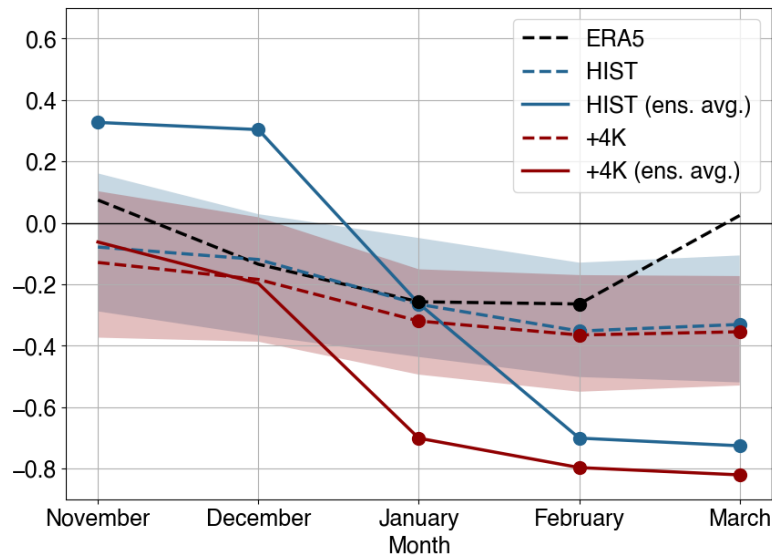


Figure 2. Temporal correlation of SLP anomalies averaged over the AL ($40^{\circ}\text{--}55^{\circ}\text{N}$, $180^{\circ}\text{--}150^{\circ}\text{W}$) and IL ($60^{\circ}\text{--}70^{\circ}\text{N}$, $40^{\circ}\text{--}10^{\circ}\text{W}$) regions for each calendar month. Shading represents the 5th-95th percentile range of d4PDF HIST (blue) and +4K (red) ensembles, with the median shown by a dashed line. The black dashed line represents the correlation based on ERA5. Solid lines represent the correlation between ensemble-averaged time series of HIST (blue) and +4K (red). Dots indicate the statistical significance at the 95% level.

This seasonality of the NAM structure and its change under global warming are linked to the AIS. Figure 2 shows the seasonality of the SLP anomaly correlation between the AL and IL regions. In ERA5, the correlation is insignificant in November and December, but negatively strengthens into late winter, becoming marginally significant in January and February (black dashed line in Figure 2). This late-winter negative correlation represents the AIS (Honda & Nakamura 2001). Since the AIS combined with the NAO can represent the NAM, the AIS seasonality is consistent with the structural seasonality of the NAM.

Except for March, d4PDF HIST experiment captures the observed AIS within the ensemble spread, demonstrating the capability of d4PDF to reproduce the NAM seasonality (blue shading in Figure 2). The intraseasonal change of the correlation is more remarkable in the ensemble mean (blue solid line in Figure 2), the component driven by the forcings external to the atmosphere, namely SST and sea ice variability. In the HIST ensemble mean, the AL-IL correlation is significantly positive in early winter (November and December), but turns significantly negative in late winter (January and beyond).

In the +4K ensemble mean, the AL-IL correlation is more negative than in HIST throughout the cold season, with a negative correlation already in December (red solid line in Figure 2). The stronger negative correlation is also found in the all-member variability in +4K compared to HIST in each calendar month (red shading in Figure 2). The disappearance of subseasonal compensation and the strengthening of AL-IL correlation contribute to the structural changes of the seasonally averaged NAM under global warming.

3.2 Externally forced component of the NAM

Next, we evaluate the externally (sea surface-) driven component of the NAM as the d4PDF ensemble mean. The AL anomaly of the externally driven NAM strengthens from December to February in both HIST and +4K (Figure S2). In December, the AL anomaly is almost missing in HIST but obvious in +4K. This is consistent with the AIS emergence in early winter in the warmer climate (Figure 2).

Table 1. Statistical properties of the NAM index. The ratio of the externally forced variance to total variance of the NAM index (evaluated following Rowell et al., (1995)) and the correlation between the ensemble-averaged NAM and the Niño 3.4 indices. Asterisks and daggers indicate the 95% statistical significance of the non-zero correlations and their difference from those of HIST, respectively.

	Ratio of the ensemble-averaged NAM variance to the total variance				Correlation with the Niño 3.4 index			
	DJF	Dec	Jan	Feb	DJF	Dec	Jan	Feb
ERA5	-	-	-	-	-0.06	0.15	-0.12	-0.18
d4PDF HIST	9.5%	3.8%	4.8%	10.2%	-0.18*	0.06*	-0.09*	-0.24*
d4PDF +4K	31.0%	8.0%	17.3%	21.0%	-0.50* [†]	-0.21* [†]	-0.36* [†]	-0.41* [†]

Under global warming, the ratio of SST/sea ice-driven variance to total variance of the NAM increases. In HIST, this ratio increases from early to late winter (d4PDF HIST of Table 1), corresponding to the late winter emergence of the AIS. In +4K, this ratio more than doubles in each calendar month compared with HIST (d4PDF +4K in Table 1). In the DJF mean, the ratio increases more than threefold, since the intraseasonal compensation of the AL-IL correlation in HIST disappears in +4K (Figure 2). These results suggest that the potential predictability of the

NAM increases under global warming. While the separate NAM definitions for HIST and +4K might raise a concern of mixing up differences in spatial patterns and temporal behaviors, our additional analyses with common spatial patterns confirm the robustness of the result (Table S1).

We also estimate the required ensemble size for robust signal detection. Following Mori et al. (2014), we perform a bootstrap sampling from the ensembles of HIST and +4K and obtain the NAM index from the subsampled members for the DJF mean variability (Figure S3). The 5th-95th percentile range is well separated with 10 or more members. For individual calendar months, 50 and 20 or more members are required for December and February, respectively (Figures not shown). It is noteworthy that our result is based on ensemble simulations of a single AGCM, and thus the above members can be considered as the lower limits. The required ensemble size can be even larger when the analysis is based on multi-model ensemble simulations.

3.3 ENSO teleconnection contributing to the seasonality

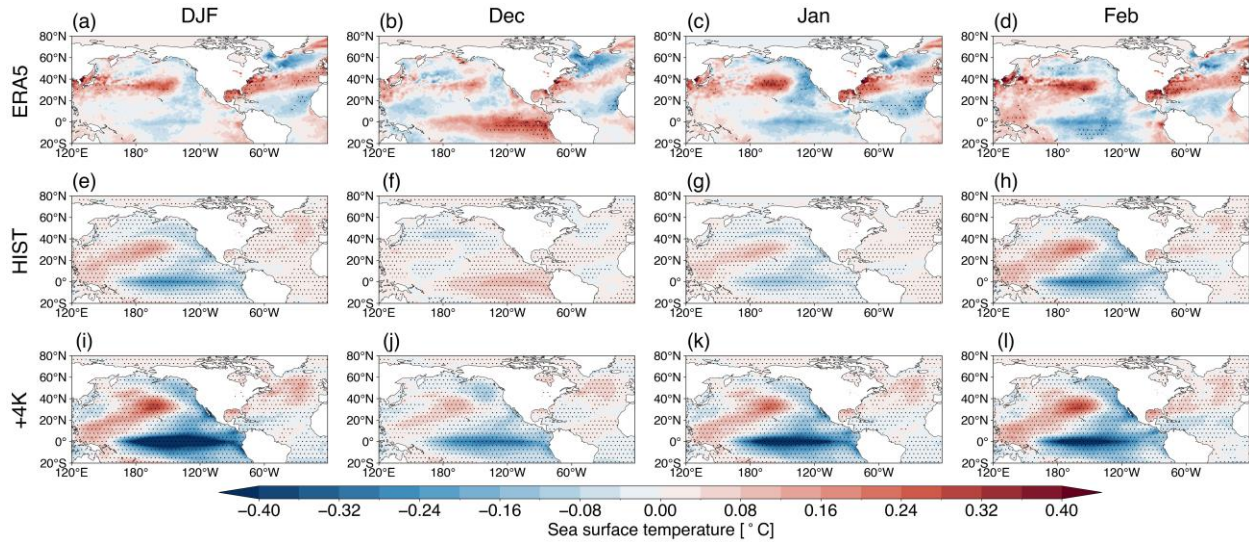


Figure 3. Same as Figure 1, but SST anomalies ($^{\circ}\text{C}$) are regressed onto the NAM index.

We investigate the SST variability correlated with the NAM (Figure 3). In HIST, a distinct polarity change in SST anomalies is evident over the equatorial Pacific from December to February (Figures 3f-h), indicating that the positive NAM is associated with El Niño in December but with La Niña in February. This intraseasonal reversal is also found based on the NAO (Moron & Gouirand, 2003). In the warmer climate, in contrast, the polarity in December changes, and the positive NAM is consistently associated with La Niña throughout winter. These results suggest that the El Niño-Southern Oscillation (ENSO) is an important driver for the NAM regarding both seasonality and changes under global warming.

Table 1 also shows the correlation of the NAM index with the Niño 3.4 index (the detrended SST anomalies over the Niño 3.4 region, common to HIST and +4K). In HIST, the NAM-ENSO correlation is positive and marginally significant in December and then transitions to significant negative values in January and February, consistent with ERA5. In +4K, the correlation becomes more negative, with a December value comparable to the HIST late-winter values. Again, these results are robust against the different definitions of the NAM index (Table S1).

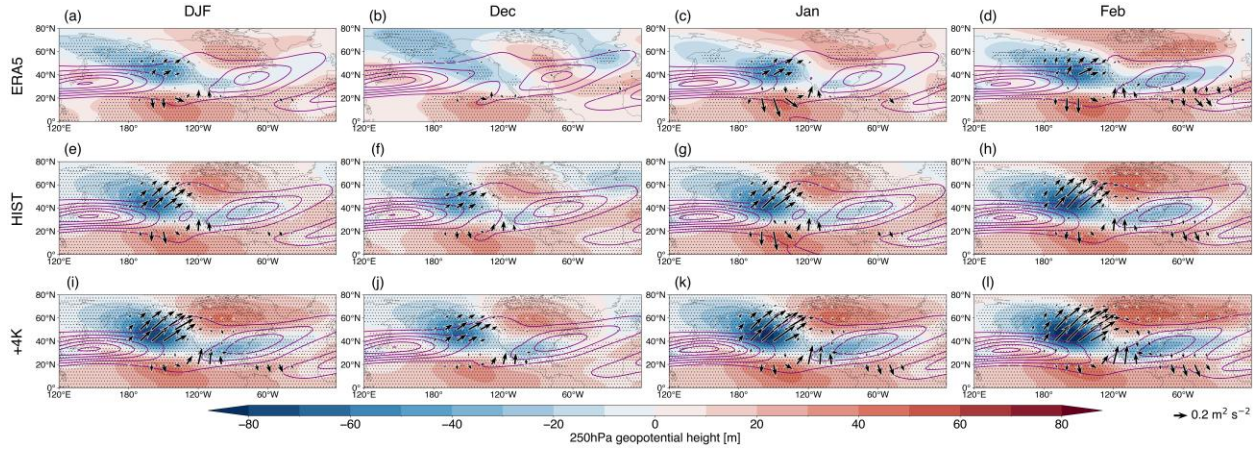


Figure 4. Z250 anomalies (shading, m) regressed onto the normalized Niño 3.4 index for (a) DJF-mean, (b) December, (c) January, and (d) February based on ERA5. (e-h) and (i-l) are the same as (a-d), but for d4PDF HIST and +4K, respectively. Arrows indicate the associated wave activity flux ($\text{m}^2 \text{s}^{-2}$; Takaya & Nakamura, 2001). Solid lines indicate climatological zonal wind (5 m s^{-1} interval from 20 m s^{-1}). Dots indicate the statistical significance at the 95% level.

To understand the seasonality of the NAM-ENSO correlation and its changes under global warming, we compare the ensemble-averaged 250 hPa geopotential height anomalies regressed onto the Niño 3.4 index among ERA5, HIST, and +4K (Figure 4). A wavetrain pattern emanating from the climatological jet exit over the Northeastern Pacific and extending eastward through North America into the North Atlantic is evident in HIST, reproducing the observational counterpart. In December of HIST, its downstream extension projects onto the positive NAO over the North Atlantic, yielding the same-sign anomalies between the AL and IL. This is consistent with the significant in-phase relationship between the two lows in December (blue solid line in Figure 2) and the marginally significant positive correlation between NAM and ENSO (Table 1). In February of HIST, by contrast, a meridional pair of positive and negative anomalies extending eastward from North America into the Atlantic projects onto the negative NAO, reflecting the seasonality of ENSO-NAO teleconnection (Abid et al., 2021; Geng et al., 2023). Consequently, the AL and IL anomalies have the opposite sign, and the NAM-ENSO correlation becomes negative.

In +4K, the meridional pair of the ENSO-related December height anomalies over North America is stronger and elongated farther eastward than its HIST counterpart, resembling the mid-to-late-winter pattern in HIST over North America and the North Atlantic (Figures 4g and 4j). This negative NAO-like pattern results in the AIS appearance even in early winter. This also means a disappearance of the intraseasonal ENSO-NAO teleconnection reversal under global warming, which is consistent with Geng et al. (2024). Furthermore, the negative NAM-ENSO correlation in mid- to late winter strengthens. Consequently, there is a significant enhancement of the negative NAM-ENSO correlation in the DJF average (Table 1).

4 Discussions

One of the possible mechanisms for the strengthening of the NAM-ENSO correlation is the change in convective activity anomalies associated with ENSO under global warming (Power et

al., 2013; Yeh et al., 2018). In +4K, the ENSO convective anomalies are enhanced in the tropical Pacific, especially in its eastern portion, compared to HIST (Figure S4). The latter change acts to shift the ENSO-forced Rossby wavetrain eastward and better project onto the NAO in the opposite polarity with ENSO. This interpretation is consistent with previous studies (Drouard & Cassou, 2019; Kug et al., 2010). It should be noted that, since the structure and magnitude of ENSO's SST anomalies are the same between the HIST and +4K experiments, the change in atmospheric response is attributable to the background changes associated with global warming.

Besides, changes in the background jet stream due to global warming may affect the teleconnection of ENSO. Figure 4 suggests a Rossby wave propagation pathway from the Pacific midlatitude jet and another pathway from the subtropical Northeastern Pacific through Central America to the North Atlantic. The +4K experiment indicates that the westerly winds strengthen over the Northeastern Pacific and better connect the jets of the two ocean basins (Figure S5). This implies an enhanced propagation of Rossby waves from the Pacific to the Atlantic (Drouard & Cassou, 2019). A detailed investigation to verify this hypothesis is left for future work.

The above hypotheses depend on the spatial pattern of SST warming. For each of the six warming patterns imposed to +4K (Figure S1), we separately define the NAM index by the same procedure and evaluate the NAM-ENSO correlation. We focus on the pattern of equatorial Pacific warming, namely whether it is El Niño-like or not. Figure S6 examines the relationship between the climatological equatorial Pacific zonal SST gradient change and the correlation of the ensemble-averaged NAM with ENSO in December. Although the sample size is small, a negative inter-warming pattern correlation is clear, where the El Niño-like warming pattern tends to have a stronger NAM-ENSO correlation. The El Niño-like background SST warming causes the eastward shift of the ENSO convection anomalies (Bayr et al., 2014), letting the ENSO teleconnection reach farther eastward. Besides, El Niño-like SST warming leads to deepening the climatological AL and accelerating the Pacific jet stream (Gan et al., 2017), which can enhance the teleconnection toward the North Atlantic.

5 Conclusions

This study investigates the NAM seasonality and its modulations under global warming, using a large ensemble AGCM simulation dataset d4PDF. The HIST experiment confirms that the AL anomaly associated with NAM strengthens from early to late winter (Figures 1e-h). We show an enhanced AL anomaly throughout winter in a warmer climate (Figures 1i-l). This change is related to the seasonally earlier emergence and strengthening of the AIS (Figure 2). Our results demonstrate that the ENSO teleconnection reaches farther eastward with global warming and changes the AIS seasonality and strength (Figure 4, Table 1). The linkage between NAM and ENSO strengthens, leading to the increased proportion of NAM variance driven by SST and sea ice variability (Figure 3, Table 1).

The modulation in the NAM under global warming is similar to the change from early to late winter. In the historical climate, the NAM seasonality is affected by a contrasting ENSO-NAO teleconnection between early and late winter. Global warming leads to a seasonally consistent ENSO-NAO correlation, altering the NAM more like the late winter situation in the present climate.

It should be noted that this study benefits from the use of a single AGCM large ensemble. First, the ensemble average represents the component driven by SST and sea ice variability. Evaluation of the influence of sea surface condition variability on total NAM variance is thus straightforward. Second, since SST variability is common between HIST and +4K, any change in NAM variability is attributable to changes in the background condition. Yet, validation is necessary to determine whether these results are robust in other models. In particular, it is worth investigating whether the NAM changes identified in this study are common in other AGCMs and whether they are robust against diverse changes in ENSO's SST anomalies in coupled models.

Acknowledgments

The authors thank Mr. Kento Usui (The University of Tokyo) for his help in the initial stage of this study. This work is supported by the Japan Ministry of Education, Culture, Sports, Science, and Technology through the advanced studies of climate change projection (SENTAN: Grant Number JPMXD0722680395) program, the Arctic Challenge for Sustainability II (ArCS II: Grant Number JPMXD1420318865) Program, by the Japan Society for the Promotion of Science through KAKENHI Grant Numbers JP19H05703, JP23K22570, JP23K25937, JP23K25946, and JP24H02223, by the Environment Research and Technology Development Fund (JPMEERF20242001) of the Environmental Restoration and Conservation Agency provided by Ministry of the Environment of Japan, and by International Graduate Program for Excellence in Earth-Space Science (IGPEES), a World-leading Innovative Graduate Study (WINGS) Program, the University of Tokyo.

Data Availability Statement

The d4PDF dataset (Mizuta et al., 2017) used in this study is available through the Data Integration and Analysis System Program (DIAS) repository (via <https://diasjp.net/en/service/d4pdf-data-download/>). The ERA5 dataset (Hersbach et al., 2020) used in this study is available online (via <https://doi.org/10.24381/cds.6860a573>). The COBE-SST2 dataset (Hirahara et al., 2014) used in this study is available online (via <https://psl.noaa.gov/data/gridded/data.cobe2.html>).

References

- Abid, M. A., Kucharski, F., Molteni, F., Kang, I.-S., Tompkins, A. M., & Almazroui, M. (2021). Separating the Indian and Pacific Ocean Impacts on the Euro-Atlantic Response to ENSO and Its Transition from Early to Late Winter. *Journal of Climate*, 34(4), 1531–1548. <https://doi.org/10.1175/JCLI-D-20-0075.1>
- Ambaum, M. H. P., Hoskins, B. J., & Stephenson, D. B. (2001). Arctic Oscillation or North Atlantic Oscillation? *Journal of Climate*, 14(16), 3495–3507. [https://doi.org/10.1175/1520-0442\(2001\)014<3495:AOONAO>2.0.CO;2](https://doi.org/10.1175/1520-0442(2001)014<3495:AOONAO>2.0.CO;2)
- Baldwin, M. P., & Dunkerton, T. J. (1999). Propagation of the Arctic Oscillation from the stratosphere to the troposphere. *Journal of Geophysical Research: Atmospheres*, 104(D24), 30937–30946. <https://doi.org/10.1029/1999JD900445>
- Bayr, T., Dommenges, D., Martin, T., & Power, S. B. (2014). The eastward shift of the Walker Circulation in response to global warming and its relationship to ENSO variability. *Climate Dynamics*, 43(9), 2747–2763. <https://doi.org/10.1007/s00382-014-2091-y>

- Bretherton, C. S., Widmann, M., Dymnikov, V. P., Wallace, J. M., & Bladé, I. (1999). The Effective Number of Spatial Degrees of Freedom of a Time-Varying Field. *Journal of Climate*, 12(7), 1990–2009. [https://doi.org/10.1175/1520-0442\(1999\)012<1990:TENOSD>2.0.CO;2](https://doi.org/10.1175/1520-0442(1999)012<1990:TENOSD>2.0.CO;2)
- Coburn, J., & Pryor, S. C. (2021). Differential Credibility of Climate Modes in CMIP6. *Journal of Climate*, 34(20), 8145–8164. <https://doi.org/10.1175/JCLI-D-21-0359.1>
- Deser, C. (2000). On the teleconnectivity of the “Arctic Oscillation.” *Geophysical Research Letters*, 27(6), 779–782. <https://doi.org/10.1029/1999GL010945>
- Drouard, M., & Cassou, C. (2019). A Modeling- and Process-Oriented Study to Investigate the Projected Change of ENSO-Forced Wintertime Teleconnectivity in a Warmer World. *Journal of Climate*, 32(23), 8047–8068. <https://doi.org/10.1175/JCLI-D-18-0803.1>
- Gan, B., Wu, L., Jia, F., Li, S., Cai, W., Nakamura, H., et al. (2017). On the Response of the Aleutian Low to Greenhouse Warming. *Journal of Climate*, 30(10), 3907–3925. <https://doi.org/10.1175/JCLI-D-15-0789.1>
- Geng, X., Zhao, J., & Kug, J.-S. (2023). ENSO-driven abrupt phase shift in North Atlantic oscillation in early January. *Npj Climate and Atmospheric Science*, 6(1), 1–8. <https://doi.org/10.1038/s41612-023-00414-2>
- Geng, X., Kug, J.-S., & Kosaka, Y. (2024). Future changes in the wintertime ENSO-NAO teleconnection under greenhouse warming. *Npj Climate and Atmospheric Science*, 7(1), 1–12. <https://doi.org/10.1038/s41612-024-00627-z>
- Gong, H., Wang, L., Chen, W., Chen, X., & Nath, D. (2017). Biases of the wintertime Arctic Oscillation in CMIP5 models. *Environmental Research Letters*, 12(1), 014001. <https://doi.org/10.1088/1748-9326/12/1/014001>
- Hamouda, M. E., Pasquero, C., & Tziperman, E. (2021). Decoupling of the Arctic Oscillation and North Atlantic Oscillation in a warmer climate. *Nature Climate Change*, 11(2), 137–142. <https://doi.org/10.1038/s41558-020-00966-8>
- He, S., Gao, Y., Li, F., Wang, H., & He, Y. (2017). Impact of Arctic Oscillation on the East Asian climate: A review. *Earth-Science Reviews*, 164, 48–62. <https://doi.org/10.1016/j.earscirev.2016.10.014>
- Hersbach, H., Bell, B., Berrisford, P., Hirahara, S., Horányi, A., Muñoz-Sabater, J., et al. (2020). The ERA5 global reanalysis. *Quarterly Journal of the Royal Meteorological Society*, 146(730), 1999–2049. <https://doi.org/10.1002/qj.3803>
- Hirahara, S., Ishii, M., & Fukuda, Y. (2014). Centennial-Scale Sea Surface Temperature Analysis and Its Uncertainty. *Journal of Climate*, 27(1), 57–75. <https://doi.org/10.1175/JCLI-D-12-00837.1>
- Honda, M., & Nakamura, H. (2001). Interannual Seesaw between the Aleutian and Icelandic Lows. Part II: Its Significance in the Interannual Variability over the Wintertime Northern Hemisphere. *Journal of Climate*, 14(24), 4512–4529. [https://doi.org/10.1175/1520-0442\(2001\)014<4512:ISBTAA>2.0.CO;2](https://doi.org/10.1175/1520-0442(2001)014<4512:ISBTAA>2.0.CO;2)
- Kidston, J., Scaife, A. A., Hardiman, S. C., Mitchell, D. M., Butchart, N., Baldwin, M. P., & Gray, L. J. (2015). Stratospheric influence on tropospheric jet streams, storm tracks and surface weather. *Nature Geoscience*, 8(6), 433–440. <https://doi.org/10.1038/ngeo2424>
- Kug, J.-S., An, S.-I., Ham, Y.-G., & Kang, I.-S. (2010). Changes in El Niño and La Niña teleconnections over North Pacific–America in the global warming simulations. *Theoretical and Applied Climatology*, 100(3), 275–282. <https://doi.org/10.1007/s00704-009-0183-0>
- Lee, J.-Y., Marotzke, J., Bala, G., Cao, L., Corti, S., Dunne, J. P., et al. (2021). Future global climate: scenario-based projections and near-term information. In V. Masson-Delmotte, P. Zhai,

- A. Pirani, S. L. Connors, C. Péan, S. Berger, et al. (Eds.), *Climate Change 2021: The Physical Science Basis. Contribution of Working Group I to the Sixth Assessment Report of the Intergovernmental Panel on Climate Change* (pp. 553–672). Cambridge, United Kingdom and New York, NY, USA: Cambridge University Press. <https://doi.org/10.1017/9781009157896.001>
- Mizuta, R., Murata, A., Ishii, M., Shiogama, H., Hibino, K., Mori, N., et al. (2017). Over 5,000 Years of Ensemble Future Climate Simulations by 60-km Global and 20-km Regional Atmospheric Models. *Bulletin of the American Meteorological Society*, 98(7), 1383–1398. <https://doi.org/10.1175/BAMS-D-16-0099.1>
- Mori, M., Watanabe, M., Shiogama, H., Inoue, J., & Kimoto, M. (2014). Robust Arctic sea-ice influence on the frequent Eurasian cold winters in past decades. *Nature Geoscience*, 7(12), 869–873. <https://doi.org/10.1038/ngeo2277>
- Moron, V., & Gouirand, I. (2003). Seasonal modulation of the El Niño–southern oscillation relationship with sea level pressure anomalies over the North Atlantic in October–March 1873–1996. *International Journal of Climatology*, 23(2), 143–155. <https://doi.org/10.1002/joc.868>
- Power, S., Delage, F., Chung, C., Kociuba, G., & Keay, K. (2013). Robust twenty-first-century projections of El Niño and related precipitation variability. *Nature*, 502(7472), 541–545. <https://doi.org/10.1038/nature12580>
- Rowell, D. P., Folland, C. K., Maskell, K., & Ward, M. N. (1995). Variability of summer rainfall over tropical north Africa (1906–92): Observations and modelling. *Quarterly Journal of the Royal Meteorological Society*, 121(523), 669–704. <https://doi.org/10.1002/qj.49712152311>
- Takaya, K., & Nakamura, H. (2001). A Formulation of a Phase-Independent Wave-Activity Flux for Stationary and Migratory Quasigeostrophic Eddies on a Zonally Varying Basic Flow. *Journal of the Atmospheric Sciences*, 58(6), 608–627. [https://doi.org/10.1175/1520-0469\(2001\)058<0608:AFOAPI>2.0.CO;2](https://doi.org/10.1175/1520-0469(2001)058<0608:AFOAPI>2.0.CO;2)
- Taylor, K. E., Stouffer, R. J., & Meehl, G. A. (2012). An Overview of CMIP5 and the Experiment Design. *Bulletin of the American Meteorological Society*, 93(4), 485–498. <https://doi.org/10.1175/BAMS-D-11-00094.1>
- Thompson, D. W. J., & Wallace, J. M. (1998). The Arctic oscillation signature in the wintertime geopotential height and temperature fields. *Geophysical Research Letters*, 25(9), 1297–1300. <https://doi.org/10.1029/98GL00950>
- Thompson, D. W. J., & Wallace, J. M. (2000). Annular modes in the extratropical circulation. Part I: Month-to-month variability. *Journal of Climate*, 13(5), 1000–1016.
- Wallace, J. M. (2000). North atlantic oscillation annular mode: Two paradigms—one phenomenon. *Quarterly Journal of the Royal Meteorological Society*, 126(564), 791–805. <https://doi.org/10.1002/qj.49712656402>
- Yeh, S.-W., Cai, W., Min, S.-K., McPhaden, M. J., Dommenges, D., Dewitte, B., et al. (2018). ENSO Atmospheric Teleconnections and Their Response to Greenhouse Gas Forcing. *Reviews of Geophysics*, 56(1), 185–206. <https://doi.org/10.1002/2017RG000568>
- Zuo, J.-Q., Li, W.-J., & Ren, H.-L. (2013). Representation of the Arctic Oscillation in the CMIP5 Models. *Advances in Climate Change Research*, 4(4), 242–249. <https://doi.org/10.3724/SP.J.1248.2013.242>